Itzhack Y. Bar-Itzhack Memorial Symposium on Estimation, Navigation, and Spacecraft Control, Haifa, Israel, October 14–17, 2012

Time-Critical Cooperative Path Following of Multiple UAVs: Case Studies

Isaac Kaminer*
Naval Postgraduate School, Monterey, CA 93943, United States

Enric Xargay†, Venanzio Cichella‡, and Naira Hovakimyan§
University of Illinois at Urbana-Champaign, Urbana, IL 61801, United States

António M. Pascoal¶ and A. Pedro Aguiar ‖
Instituto Superior Técnico, Technical University of Lisbon, LX 1049, Portugal

Vladimir Dobrokhodov**
Naval Postgraduate School, Monterey, CA 93943, United States

Reza Ghabcheloo††
Tampere University of Technology, Tampere, FI-33101, Finland

This paper describes a multi-vehicle motion control framework for time-critical cooperative missions and evaluates its performance by considering two case studies: a simultaneous arrival mission scenario and a sequential auto-landing of a fleet of UAVs. In the adopted setup, the UAVs are assigned nominal spatial paths and speed profiles along those, and the vehicles are then tasked to execute cooperative path following, rather than "open-loop" trajectory-tracking maneuvers. This cooperative strategy yields robust behavior against external disturbances by allowing the UAVs to negotiate their speeds along the paths in response to coordination information exchanged over the supporting communications network. The approach applies to teams of heterogeneous vehicles and does not necessarily lead to swarming behavior.

I. Introduction

Unmanned Aerial Vehicles (UAVs) are ubiquitous in military reconnaissance and strike operations, border patrol missions, forest fire detection, police surveillance, and recovery operations. In simple applications, a single autonomous vehicle can be managed by a crew using a ground station provided by the vehicle manufacturer. The execution of more challenging missions, however, requires the use of multiple vehicles working in cooperation to achieve a common objective. Representative examples of cooperative mission

*Professor, Department of Mechanical & Astronautical Engineering, kaminer@nps.edu.
†PhD Candidate, Department of Aerospace Engineering, xargay@illinois.edu.
‡PhD Student, Department of Mechanical Science & Engineering, cichell2@illinois.edu.
§Professor, Department of Mechanical Science & Engineering, nhovakim@illinois.edu.
¶Associate Professor, Laboratory of Robotics and Systems in Engineering and Science (LARSyS), antonio@isr.ist.utl.pt.
‖Assistant Professor, Laboratory of Robotics and Systems in Engineering and Science (LARSyS), pedro@isr.ist.utl.pt.
**Research Associate Professor, Department of Mechanical & Astronautical Engineering, vldobr@nps.edu.
††Research Fellow, Department of Intelligent Hydraulics and Automation, reza.ghabcheloo@tut.fi.

scenarios are sequential auto-landing and coordinated ground target suppression for multiple UAVs. In both cases, only *relative* (rather than *absolute*) temporal constraints are given a priori, and the vehicles must execute maneuvers in close proximity to each other. Also, the information exchanged among vehicles may be restricted for security reasons or because of tight bandwidth limitations. Moreover, the topology of the inter-vehicle communications network supporting the cooperative mission may change over time. This paper considers cooperative motion control strategies that can yield robust performance in the presence of time-varying communications networks arising from temporary loss of communications links and switching communications topologies.

The range of relevant, related topics addressed in literature includes parallel computing [1], synchronization of oscillators [2], study of collective behavior and flocking [3], multi-system consensus mechanisms [4], multi-vehicle system formations [5–8], coordinated motion control [9–11], cooperative path and trajectory planning [12–16], asynchronous protocols [17], dynamic graphs [18], stochastic graphs [18–20], and graph-related theory [21,22]. Especially relevant are the applications of the theory developed in the area of multi-vehicle formation control: spacecraft formation flying [23], UAV control [24,25], coordinated control of land robots [9], and control of multiple autonomous underwater vehicles and surface vessels [26–35]. In spite of significant progress in the field, much work remains to be done to develop strategies capable of yielding robust performance of a fleet of vehicles in the presence of complex vehicle dynamics, communications constraints, and partial vehicle failures.

In [36], we addressed the problem of *steering a fleet of UAVs along desired paths while meeting stringent spatial and temporal constraints*. The vehicles are assigned nominal paths and speed profiles along them, obtained form the solution of an appropriately formulated optimization problem for the given mission. The paths are appropriately parameterized, and the vehicles are requested to execute cooperative path following, rather than "open-loop" trajectory-tracking maneuvers. The strategies derived yield robust performance in the face of external disturbances by allowing the vehicles to negotiate their speeds along the paths in response to information exchanged over the supporting communications network. The proposed solution has a multiloop control structure in which an inner-loop controller stabilizes the vehicle dynamics, while a guidance outer-loop controller is designed to control the vehicle kinematics, providing path-following and time-coordination capabilities. This inner-outer loop approach simplifies the design process and affords the designer a systematic approach to seamlessly tailor the algorithms for a very general class of vehicles that come equipped with inner-loop commercial autopilots. The reader is referred to [37–42] and the references therein for a general perspective of key ideas and concepts that are at the root of this cooperative approach.

In the present paper, we present simulation results of two multi-vehicle time-critical missions that exploit the cooperative control framework developed in [36]. In the first mission, three UAVs must follow spatially-deconflicted paths and arrive at predefined locations at the same time. The second mission considers the case of sequential auto-landing, in which three UAVs must arrive at the glide path separated by prespecified safe-guarding time-intervals and maintain this separation as they fly along the glideslope. In this second scenario, the cooperative control algorithm is critical to provide UAV trajectory deconfliction, as well as to ensure that the UAVs follow the glide path at a desired approach speed while maintaining the safe-guarding separation.

The paper is organized as follows. Section II formulates the time-critical cooperative path-following problem, describes the kinematics of the systems of interest, and introduces

a set of assumptions on the supporting communications network. Section III presents a path-following control algorithm for UAVs in 3D space. Section IV derives a strategy for time-critical cooperative path following of multiple UAVs that relies on the adjustment of the speed profile of each vehicle. This section also discusses the convergence properties of the overall control architecture. Section V presents simulation results that demonstrate the effectiveness of the algorithms. Finally, Section VI summarizes the key results and contains the main conclusions.

Notation

The following notation is used throughout the paper. $\{v\}_F$ is used to denote the vector v resolved in frame $\mathcal{F}$; $\{\vec{e}\}_F$ represents the vector $\vec{e}$ resolved in frame $\mathcal{F}$; $\omega_{F1/F2}$ denotes the angular velocity of frame $\mathcal{F}1$ with respect to frame $\mathcal{F}2$; the rotation matrix from frame $\mathcal{F}1$ to frame $\mathcal{F}2$ is represented by R_{F1}^{F2}; $\dot{v}\,]_F$ indicates that the time-derivative of vector v is taken in frame $\mathcal{F}$. Unless otherwise noted, $\|\cdot\|$ is used for both the 2-norm of a vector and the induced 2-norm of a matrix. Finally, $\mathsf{SO}(3)$ denotes the Special Orthogonal group of all rotations about the origin of three-dimensional Euclidean space $\mathbb{R}^3$, while $\mathfrak{so}(3)$ represents the set of 3×3 skew-symmetric matrices over $\mathbb{R}$.

II. Time-Critical Cooperative Path Following: Problem Formulation

This section provides a brief formulation of the problem of time-critical cooperative path-following control for multiple UAVs in 3D space, in which a fleet of UAVs is tasked to converge to and follow a set of desired feasible paths so as to meet spatial and temporal constraints. The section also introduces the set of assumptions and constraints on the supporting inter-vehicle communications network.

The problem of cooperative *trajectory generation* is not addressed in this paper. In fact, it is assumed that a set of desired 3D time trajectories $p_{d,i}(t_d) : \mathbb{R} \to \mathbb{R}^3$, conveniently parameterized by a single time-variable $t_d \in [0, t_d^*]$, are known for all the n UAVs involved in the cooperative mission. The variable t_d represents a *desired mission time* (distinct from the actual mission time that evolves as the mission unfolds), with t_d^* being the *desired mission duration*. For a given t_d, $p_{d,i}(t_d)$ defines the desired position of the ith UAV t_d seconds after the initiation of the cooperative mission. These time trajectories can be reparameterized in terms of path length to obtain *spatial paths* $p_{d,i}(\tau_{\ell,i}) : \mathbb{R} \to \mathbb{R}^3$ –with no temporal specifications– and the corresponding *desired speed profiles* $v_{d,i}(t_d) : \mathbb{R} \to \mathbb{R}$. For convenience, each spatial path is parameterized by its path length $\tau_{\ell,i} \in [0, \ell_{fi}]$, where ℓ_{fi} denotes the total length of the ith path, whereas the desired speed profiles are parameterized by the desired mission time t_d. It is assumed that both the paths and the speed profiles satisfy collision-avoidance constraints as well as appropriate boundary and feasibility conditions, such as those imposed by the physical limitations of the UAVs. The problem of generation of feasible collision-free trajectories for multiple cooperative autonomous vehicles is described in detail in [43].

A. Path Following for a Single UAV

Pioneering work in the area of path following can be found in [44], where an elegant solution to the problem was presented for a wheeled robot at the kinematic level. In [44], the kinematic model of the vehicle was derived with respect to a Frenet-Serret frame

moving along the path, while playing the role of a *virtual target vehicle* to be tracked by the real vehicle. The origin of the Frenet-Serret was placed at the point on the path closest to the real vehicle. This work led to a great deal of activity in the literature addressing the path-following control problem. Of particular interest is the work reported in [45], in which the authors reformulated the setup used in [44] and derived a feedback control law that steers the dynamic model of a wheeled robot along a desired path and overcomes stringent initial condition constraints present in [44]. The key to the algorithm in [45] is to explicitly control the rate of progression of the virtual target along the path. This effectively creates an extra degree of freedom that can be exploited to avoid singularities that occur when the distance to the path is not well defined.

The solution to the path-following problem described in the present paper extends the algorithm presented in [45] to the 3D case, and relies on the insight that a UAV can follow a given path using only its attitude, thus leaving its linear speed as an extra degree of freedom to be used at the coordination level. The key idea behind the algorithm is to use the vehicle's attitude control effectors to follow a virtual target vehicle running along the path. To this effect, following the approach developed in [45], this section introduces a frame attached to this virtual target and defines a generalized error vector between this moving coordinate system and a frame attached to the actual vehicle. With this setup, the path-following control problem is reduced to that of driving this generalized error vector to zero by using only the UAV's attitude control effectors, while following an arbitrary feasible speed profile. Next, the dynamics of the kinematic errors between the ith vehicle and its virtual target are described.

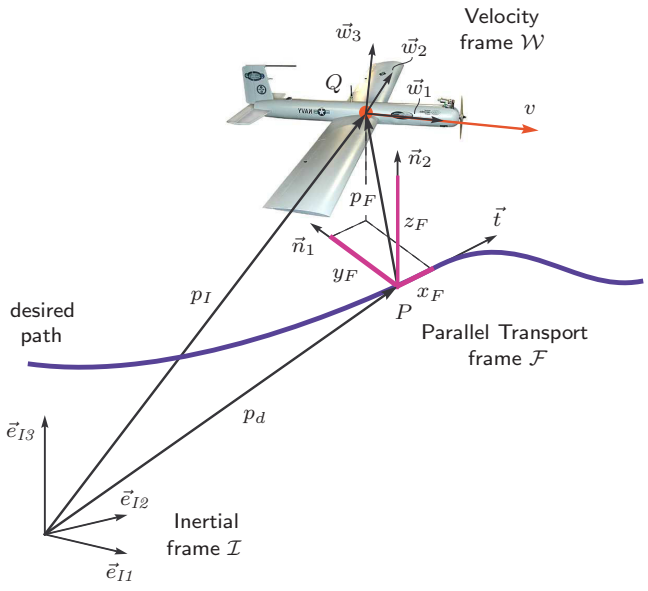

Figure 1: Following a virtual target vehicle. Problem geometry.

Figure 1 captures the geometry of the problem at hand. Let $p_d(\cdot)$ be the desired path assigned to one of the UAVs, and let ℓ_f be its total length. Let $\mathcal{I}$ denote an inertial reference frame $\{\vec{e}_{I1}, \vec{e}_{I2}, \vec{e}_{I3}\}$, and let $p_I(t)$ be the position of the center of mass Q of the UAV in this inertial frame. Further, let P be an arbitrary point on the desired path that plays the role of the virtual target, and let $p_d(\ell)$ denote its position in the inertial frame. Here $\ell \in [0, \ell_f]$ is a free length-variable that defines the position of the virtual

target vehicle along the path. In the setup adopted, the total rate of progression of the virtual target along the path is an extra design parameter. Endowing point P with an extra degree of freedom is the key to the path-following algorithm presented in [45] and its extension to the 3D case described in this paper.

For our purposes, it is convenient to define a *parallel transport frame* $\mathcal{F}$ [46, 47] attached to point P on the path and characterized by vectors $\{\vec{t}(\ell), \vec{n}_1(\ell), \vec{n}_2(\ell)\}$. Vectors $\{\vec{t}, \vec{n}_1, \vec{n}_2\}$ define an orthonormal basis for $\mathcal{F}$, in which the unit vector $\vec{t}(\ell)$ defines the tangent direction to the path at the point determined by ℓ, while $\vec{n}_1(\ell)$ and $\vec{n}_2(\ell)$ define the normal plane perpendicular to $\vec{t}(\ell)$. Unlike the Frenet-Serret frame, this moving frame is well defined when the path has a vanishing second derivative. Moreover, let $p_F(t)$ be the position of the vehicle's center of mass Q in the parallel transport frame, and let $x_F(t)$, $y_F(t)$, and $z_F(t)$ be the components of the vector $p_F(t)$ with respect to the basis $\{\vec{t}, \vec{n}_1, \vec{n}_2\}$.

Let $\mathcal{W}$ denote a vehicle-carried *velocity frame* $\{\vec{w}_1, \vec{w}_2, \vec{w}_3\}$ with its origin at the UAV center of mass and its x-axis aligned with the velocity vector of the UAV. The z-axis is chosen to lie in the plane of symmetry of the UAV, and the y-axis is determined by completing the right-hand system. In this paper, $q(t)$ and $r(t)$ are the y-axis and z-axis components, respectively, of the vehicle's rotational velocity resolved in the $\mathcal{W}$ frame. With a slight abuse of notation, $q(t)$ and $r(t)$ will be referred to as *pitch rate* and *yaw rate*, respectively, in the $\mathcal{W}$ frame.

We also introduce an auxiliary frame $\mathcal{D}$ $\{\vec{b}_{1D}, \vec{b}_{2D}, \vec{b}_{3D}\}$, which is used to shape the approach attitude to the path as a function of the cross-track error components y_F and z_F. Frame $\mathcal{D}$ has its origin at the UAV center of mass and the vectors $\vec{b}_{1D}(t)$, $\vec{b}_{2D}(t)$, and $\vec{b}_{3D}(t)$ are defined as

$$\vec{b}_{1D} \triangleq \frac{d\,\vec{t} - y_F\,\vec{n}_1 - z_F\,\vec{n}_2}{(d^2 + y_F^2 + z_F^2)^{\frac{1}{2}}}, \qquad \vec{b}_{2D} \triangleq \frac{y_F\,\vec{t} + d\,\vec{n}_1}{(d^2 + y_F^2)^{\frac{1}{2}}}, \qquad \vec{b}_{3D} \triangleq \vec{b}_{1D} \times \vec{b}_{2D}\,, \tag{1}$$

with d being a (positive) constant *characteristic distance* that plays the role of a design parameter, as will become clear later. The basis vector $\vec{b}_{1D}(t)$ defines the desired direction of the UAV's velocity vector. Clearly, when the vehicle is far from the desired path, vector $\vec{b}_{1D}(t)$ becomes perpendicular to $\vec{t}(\ell)$. As the vehicle comes closer to the path and the cross-track error becomes smaller, then $\vec{b}_{1D}(t)$ tends to $\vec{t}(\ell)$.

Finally, let $\tilde{R}(t) \in \mathsf{SO(3)}$ be the rotation matrix from $\mathcal{W}$ to $\mathcal{D}$, that is,

$$\tilde{R} \triangleq R_W^D = R_F^D\, R_W^F = (R_D^F)^\top\, R_W^F\,,$$

and define the real-valued error function on $\mathsf{SO(3)}$

$$\Psi(\tilde{R}) \triangleq \frac{1}{2}\mathrm{tr}\left[\left(\mathbb{I}_3 - \Pi_R^\top \Pi_R\right)\left(\mathbb{I}_3 - \tilde{R}\right)\right], \tag{2}$$

where Π_R is defined as $\Pi_R \triangleq \left[\begin{smallmatrix} 0 & 1 & 0 \\ 0 & 0 & 1 \end{smallmatrix}\right]$. The function $\Psi(\tilde{R})$ in (2) can be expressed in terms of the entries of $\tilde{R}(t)$ as $\Psi(\tilde{R}) = (1/2)(1 - \tilde{R}_{11})$, where $\tilde{R}_{11}(t)$ denotes the $(1,1)$ entry of $\tilde{R}(t)$. Therefore, $\Psi(\tilde{R})$ is a positive-definite function about $\tilde{R}_{11} = 1$. Note that $\tilde{R}_{11} = 1$ corresponds to the situation where the velocity vector of the UAV is aligned with the basis vector $\vec{b}_{1D}(t)$, which defines the desired attitude.

With the above notation, as shown in [36], the path-following kinematic-error dynamics between the UAV and its virtual target vehicle can be written as

$$\dot{p}_F]_F = -\,\dot{\ell}\,\vec{t}\;-\;\omega_{F/I}\times p_F\;+\;v\,\vec{w}_1\,, \tag{3}$$

$$\dot{\Psi}(\tilde{R}) = e_{\tilde{R}}\cdot\left(\begin{bmatrix} q \\ r \end{bmatrix} - \Pi_R\tilde{R}^\top\left(R_F^D\{\omega_{F/I}\}_F + \{\omega_{D/F}\}_D\right)\right)\,, \tag{4}$$

where $\cdot\,]_F$ is used to indicate that the derivative is taken in the parallel transport frame, $v(t)$ denotes the magnitude of the UAV's ground velocity vector, and $e_{\tilde{R}}(t)$ is the attitude kinematic error vector defined as

$$e_{\tilde{R}} \triangleq \frac{1}{2}\Pi_R\left(\left(\mathbb{I}_3 - \Pi_R^\top\Pi_R\right)\tilde{R} - \tilde{R}^\top\left(\mathbb{I}_3 - \Pi_R^\top\Pi_R\right)\right)^\vee\,,$$

where $(\cdot)^\vee : \mathfrak{so}(3) \to \mathbb{R}^3$ denotes the *vee map* (see Appendix). In the kinematic-error model (3)-(4), $q(t)$ and $r(t)$ play the role of control inputs, while the rate of progression $\dot{\ell}(t)$ of point P along the path becomes an extra variable that can be manipulated at will. At this point, the path-following generalized error vector $x_{pf}(t)$ can be formally defined as

$$x_{pf} \triangleq \begin{bmatrix} p_F^\top, & e_{\tilde{R}}^\top \end{bmatrix}^\top\,.$$

Notice that, within the region where $\Psi(\tilde{R}) < 1$, if $x_{pf} = 0$, then both the path-following position error and the path-following attitude error are equal to zero, that is, $p_F = 0$ and $\tilde{R}_{11} = 0$.

Using the above formulation, and given a spatially defined feasible path $p_d(\cdot)$, the problem of *path following* for a single vehicle can now be defined accodingly.

Definition 1 (Path-Following Problem) *For a given UAV (equipped with an autopilot), design feedback control laws for pitch rate $q(t)$, yaw rate $r(t)$, and rate of progression $\dot{\ell}(t)$ of the virtual target along the path such that all closed-loop signals are bounded and the path-following generalized error vector $x_{pf}(t)$ converges to a neighborhood of the origin with a guaranteed rate of convergence, regardless of what the temporal speed assignment of the mission is (as long as it is physically feasible).*

Stated in simple terms, the problem above amounts to designing feedback laws so that a UAV converges to and remains inside a tube centered on the desired path curve assigned to this UAV, for an arbitrary speed profile (subject to feasibility constraints).

B. Time-Critical Coordination and Network Model

To enforce the temporal constraints that must be met in real time to coordinate the entire fleet of vehicles, the speed profile of each vehicle is adjusted based on coordination information exchanged among the UAVs over a time-varying communications network. To solve this coordination problem, we first formulate it as a *consensus problem*, in which the objective of the fleet of vehicles is to reach an agreement on some distributed variables of interest. Hence, an appropriate coordination variable needs to be defined for each vehicle that captures the objective of the cooperative mission; in our case, simultaneous arrival of all the UAVs at their final destinations.

For this purpose, let $\ell'_{d,i}(t_d)$ be defined as the desired normalized curvilinear abscissa of the ith UAV along its corresponding path at the desired mission time t_d, which is given by

$$\ell'_{d,i}(t_d) \triangleq \frac{1}{\ell_{fi}} \int_0^{t_d} v_{d,i}(\tau)\, d\tau\,,$$

with ℓ_{fi} and $v_{d,i}(\cdot)$ being, respectively, the length of the path and the desired speed profile corresponding to the ith UAV. The trajectory-generation algorithm ensures that the desired speed profiles $v_{d,i}(\cdot)$ satisfy feasibility conditions, which implies that the following bounds hold for all vehicles:

$$0 < v_{\min} \leq v_{d,i}(\cdot) \leq v_{\max}\,, \qquad\qquad i = 1, \ldots, n\,, \tag{5}$$

where $v_{\min}$ and $v_{\max}$ denote, respectively, the minimum and maximum operating speeds of the UAVs involved in the cooperative mission. From the definition of $\ell'_{d,i}(t_d)$ and the bounds in (5), it follows that $\ell'_{d,i}(t_d)$ is a strictly increasing continuous function of t_d mapping $[0, t_d^*]$ onto $[0, 1]$, and satisfying $\ell'_{d,i}(0) = 0$ and $\ell'_{d,i}(t_d^*) = 1$. Let $\eta_i : [0, 1] \to [0, t_d^*]$ be the inverse function of $\ell'_{d,i}(t_d)$, $t_d \in [0, t_d^*]$. Clearly, $\eta_i(\cdot)$ is also a strictly increasing continuous function of its argument. Then, letting $\ell'_i(t)$ be the normalized curvilinear abscissa at time t of the ith virtual target vehicle running along its path, defined as

$$\ell'_i(t) \triangleq \frac{\ell_i(t)}{\ell_{fi}}\,,$$

where $\ell_i(t) \in [0, \ell_{fi}]$ was introduced in the previous section, define the *time*-variables

$$\xi_i(t) \triangleq \eta_i(\ell'_i(t))\,, \qquad\qquad i = 1, \ldots, n\,.$$

From this definition, it follows that $\xi(t) \in [0, t_d^*]$, and therefore this variable can be seen as a *virtual time* that characterizes the status of the mission for the ith UAV at time t in terms of the desired mission time t_d.

Note that, for any two vehicles i and j, if $\xi_i(t) = \xi_j(t) = t'_d$ at a given time t, then $\ell'_i(t) = \ell'_{d,i}(t'_d)$ and $\ell'_j(t) = \ell'_{d,j}(t'_d)$, which implies that at time t the target vehicles corresponding to UAVs i and j have the desired relative position along the path at the desired mission time t'_d. Clearly, if $\xi_i(t) = \xi_j(t)$ for all $t \geq 0$, then the ith and jth virtual target vehicles maintain desired relative position along the path at all times and, in particular, these two target vehicles arrive at their final destinations at the same time, which does not necessarily correspond to the desired mission duration t_d^*. Also, in the case of collision avoidance in time (see [43]), if $\xi_i(t) = \xi_j(t)$ for all $t \geq 0$, then the solution to the trajectory-generation problem ensures that the virtual targets i and j do not collide. Moreover, if the ith virtual target travels at the desired speed for all time in the interval $[0, t]$, that is, $\dot{\ell}_i(\tau) = v_{d,i}(\tau)$ for all $\tau \in [0, t]$, then one has that $\ell_i(\tau) = \ell_{d,i}(\tau)$ for all $\tau \in [0, t]$, which implies that $\xi_i(\tau) = \tau$ (or equivalently, that $\dot{\xi}_i(\tau) = 1$) for all $\tau \in [0, t]$. This set of properties makes the variables $\xi_i(t)$ an appropriate metric for vehicle coordination, and therefore they will be referred to as *coordination states*. Notice that the use of these specific coordination variables is motivated by the work in [40].

To meet the desired temporal assignments of the cooperative mission, coordination information is to be exchanged among the UAVs over the supporting communications network. Next, tools and facts from *algebraic graph theory* are used to model the information exchange over the time-varying network as well as the constraints imposed by the

communications topology (see, for example, [7], [48] and references therein). The reader is also referred to [49] for key concepts and details on algebraic graph theory.

First, in order to account for the communications constraints imposed by this inter-vehicle network, it is assumed that the ith UAV can only exchange information with a neighboring set of vehicles, denoted here by $\mathcal{N}_i$. It is also assumed that the communication between two UAVs is bidirectional and that the information is transmitted continuously with no delays. Moreover, since the flow of information among vehicles may be severely restricted, either for security reasons or because of tight bandwidth limitations, each vehicle is only allowed to exchange its coordination state $\xi_i(t)$ with its neighbors. Finally, it is assumed that the connectivity of the communications graph $\Gamma(t)$ that captures the underlying bidirectional communications network topology of the fleet at time t satisfies the persistency of excitation (PE)-like condition

$$\frac{1}{n}\frac{1}{T}\int_{t}^{t+T} Q\,L(\tau)\,Q^{\top}d\tau \geq \mu\,\mathbb{I}_{n-1}\,, \qquad \text{for all } t \geq 0\,, \tag{6}$$

where $L(t) \in \mathbb{R}^{n\times n}$ is the Laplacian of the graph $\Gamma(t)$, and Q is an $(n-1)\times n$ matrix such that $Q1_n = 0$ and $QQ^{\top} = \mathbb{I}_{n-1}$, with 1_n being the vector in $\mathbb{R}^n$ whose components are all 1. The parameters $T, \mu > 0$ characterize the *quality of service* (QoS) of the communications network, which in the context of this paper represents a measure of the level of connectivity of the communications graph. Note that the PE-like condition (6) requires only the communications graph $\Gamma(t)$ to be connected in an integral sense, not pointwise in time. In fact, the graph may be disconnected during some interval of time or may even fail to be connected for the entire duration of the mission. Similar types of conditions can be found, for example, in [50] and [4].

Using the formulation above, one can now define the problem of *time-critical cooperative path following* for a fleet of n UAVs.

Definition 2 (Time-Critical Cooperative Path-Following Problem) *Given a fleet of n vehicles supported by an inter-vehicle communications network and a set of desired 3D time trajectories $p_{d,i}(t_d)$, design feedback control laws for pitch rate $q(t)$, yaw rate $r(t)$, and speed $v(t)$ for all vehicles such that*

1. *all closed-loop signals remain bounded;*
2. *for each vehicle i, $i \in \{1,\ldots,n\}$, the path-following generalized error vector $x_{pf,i}(t)$ converges to a neighborhood of the origin; and*
3. *for each pair of vehicles i and j, $i,j \in \{1\ldots,n\}$, the coordination error $|\xi_i(t) - \xi_j(t)|$ converges to a neighborhood of the origin, guaranteeing (quasi-)simultaneous time of arrival and ensuring collision-free maneuvers.*

III. 3D Path Following Control law

To solve the path-following problem described in Section II.A, we first let the rate of progression of point P along the path be governed by

$$\dot{\ell} = v\,\vec{w}_1 \cdot \vec{t} + K_{\ell} p_F \cdot \vec{t}\,, \tag{7}$$

where K_ℓ is a positive constant gain. Then, the rate commands $q_c(t)$ and $r_c(t)$ given by

$$\begin{bmatrix} q_c \\ r_c \end{bmatrix} \triangleq \Pi_R \tilde{R}^\top \left(R_F^D \{\omega_{F/I}\}_F + \{\omega_{D/F}\}_D \right) \; - \; 2K_{\tilde{R}} e_{\tilde{R}}\,, \tag{8}$$

where $K_{\tilde{R}}$ is also a positive gain, drive the path-following generalized error vector $x_{pf}(t)$ to a neighborhood of zero with a guaranteed rate of convergence. More precisely, it can be shown that if the speed of the vehicle satisfies $0 < v_{\min} \leq v(t) \leq v_{\max}$, then the origin of the kinematic error equations in (3)-(4) with the controllers $q_c(t)$ and $r_c(t)$ defined in (8) is locally exponentially stable. A formal statement of this result can be found in [36].

We notice that the dynamics of the virtual target along the path depend on both the ground velocity vector of the UAV, $v\,\vec{w}_1$, and the path-following position-error vector, p_F; in fact, the first term in (7) represents the projection of the vehicle ground velocity vector onto the tangent direction to the path $\vec{t}$, while the second term corresponds to a correction related to the path-following along-track error x_F. Similarly, the rate commands in (8) also allow for an intuitive interpretation: the first term represents a feed-forward control signal that accounts for the angular velocity of frame $\mathcal{F}$ with respect to $\mathcal{I}$; the second term is responsible for shaping the approach attitude to the path as a function of the cross-track error; finally, the third term corresponds to a correction related to the path-following attitude-error $e_{\tilde{R}}$.

We also notice that the use of the Special Orthogonal group $\mathsf{SO(3)}$ in the formulation of the attitude control problem avoids the geometric singularities and complexities that appear when dealing with local parameterizations of the vehicle's attitude. See, for example, the path-following control algorithm reported in [42].

Finally, we note that the choice of the characteristic distance d in the definition of the auxiliary frame $\mathcal{D}$ (see (1)) can be used to adjust the rate of convergence of the path-following closed-loop system. This is consistent with the fact that a large parameter d reduces the penalty for cross-track position errors, which results in a slow rate of convergence of the UAV to the path. On the other hand, small values of d allow for higher rates of convergence, which however might result in oscillatory path-following behavior. Figure 2 illustrates this point.

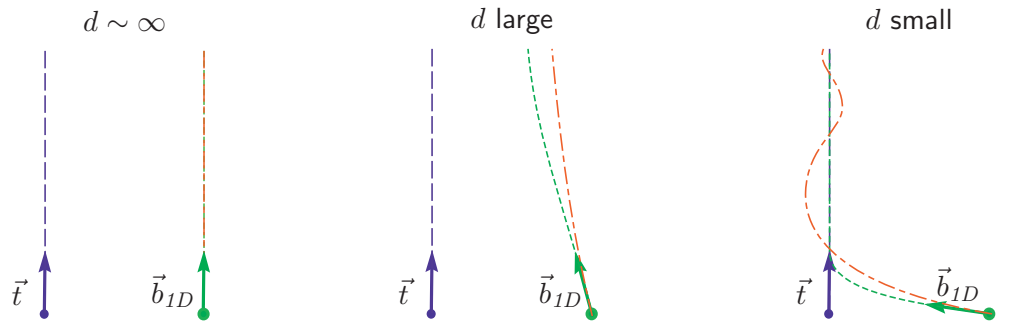

(a) no convergence (b) slow convergence (c) fast convergence

Figure 2: Effect of the characteristic distance d on the convergence of the vehicle to the path. In these plots, the blue line is the desired path, the green line represents the desired approach curve, and the red line corresponds to the resulting vehicle trajectory.

Finally, we notice that the solution to the path-following problem for the ith vehicle presented above is independent of the desired speed profile $v_{d,i}(\cdot)$, and uses only local measurements for feedback. The path-following control laws $q_c(t)$ and $r_c(t)$ represent outer-loop guidance commands that are to be tracked by the UAV to ensure safety and success of the cooperative mission. In this sense, this solution for path-following control departs from standard backstepping techniques in that the final path-following control law makes explicit use of the existing autopilot and retains its stabilizing properties and tracking capabilities.

IV. Time-Critical Coordination

The previous section presented a solution to the path-following problem for a single UAV and an arbitrary feasible speed profile by using a control strategy in which the vehicle's attitude control effectors are used to follow a virtual target running along the path. We now address the problem of time-critical cooperative path-following control of multiple vehicles. To this effect, the speeds of the UAVs are adjusted based on coordination information exchanged among the vehicles over the supporting communications network. In particular, the outer-loop coordination control law is intended to provide a correction to the desired speed profile $v_{d,i}(\cdot)$ obtained in the trajectory-generation step, and to generate a total speed command $v_{c,i}(t)$. This speed command is then to be tracked by the ith vehicle to achieve coordination in time.

A. Distributed Coordination Law

We start by noting that the evolution of the ith coordination state is given by [36]

$$\dot{\xi}_i(t) = \frac{\dot{\ell}_i(t)}{v_{d,i}(\xi_i(t))}\,.$$

Recalling from the solution to the path-following problem that the evolution of the ith virtual target vehicle along the path is described by

$$\dot{\ell}_i = (v_i\,\vec{w}_{1,i} + K_\ell\,p_{F,i})\cdot\vec{t}_i\,,$$

where for simplicity we keep K_ℓ without indexing and drop the dependency of the various variables on t, the dynamics of the ith coordination state can be rewritten as

$$\dot{\xi}_i = \frac{(v_i\,\vec{w}_{1,i} + K_\ell\,p_{F,i})\cdot\vec{t}_i}{v_{d,i}(\xi_i)}\,. \tag{9}$$

Then, to solve the time-coordination problem we use dynamic inversion and define the speed command for the ith vehicle as

$$v_{c,i} \triangleq \frac{u_{\text{coord},i}\,v_{d,i}(\xi_i) - K_\ell\,p_{F,i}\cdot\vec{t}_i}{\vec{w}_{1,i}\cdot\vec{t}_i}\,, \tag{10}$$

where $u_{\text{coord},i}(t)$ is a coordination control law to be defined later. With this speed command, the coordination dynamics for the ith target vehicle can be rewritten as

$$\dot{\xi}_i = u_{\text{coord},i} + \frac{e_{v,i}}{v_{d,i}(\xi_i)}\,\vec{w}_{1,i}\cdot\vec{t}_i\,,$$

where $e_{v,i}(t) \triangleq v_i(t) - v_{c,i}(t)$ denotes the speed tracking error for the ith UAV.

Recall now that each UAV is allowed to exchange only its coordination parameter $\xi_i(t)$ with its neighbors $\mathcal{N}_i$, which are defined by the time-varying communications topology. To observe this constraint, the following distributed coordination law is proposed:

$$u_{\text{coord},1}(t) = -a \sum_{j \in \mathcal{N}_1} (\xi_1(t) - \xi_j(t)) + 1 \,, \tag{11a}$$

$$u_{\text{coord},i}(t) = -a \sum_{j \in \mathcal{N}_i} (\xi_i(t) - \xi_j(t)) + \chi_{I,i}(t) \,, \qquad i = 2, \ldots, n \,, \tag{11b}$$

$$\dot{\chi}_{I,i}(t) = -b \sum_{j \in \mathcal{N}_i} (\xi_i(t) - \xi_j(t)) \,, \qquad \chi_{I,i}(0) = 1 \,, \qquad i = 2, \ldots, n \,, \tag{11c}$$

where vehicle 1 is elected as the formation leader (which can be a *virtual vehicle*), and a and b are positive adjustable coordination control gains. Note that the coordination control law has a proportional-integral structure, which provides disturbance rejection capabilities at the coordination level. Moreover, note that the vehicles exchange information only about the corresponding virtual targets, rather than exchanging their own state information. Finally, we notice that protocol (11) can be easily modified to include multiple leaders, which improves robustness of the control architecture to a single-point failure; see [51].

B. Overall Time-Critical Cooperative Path-Following System

Figure 3 shows the complete time-critical cooperative path-following closed-loop control architecture for the ith vehicle, including the nonlinear path-following algorithm and the distributed coordination control law. With this approach, the overall cooperative control architecture presented in this article exhibits a multiloop control structure in which an inner-loop controller stabilizes the vehicle dynamics, while guidance outer-loop controllers are designed to control the vehicle kinematics, providing path-following and time-critical cooperative capabilities.

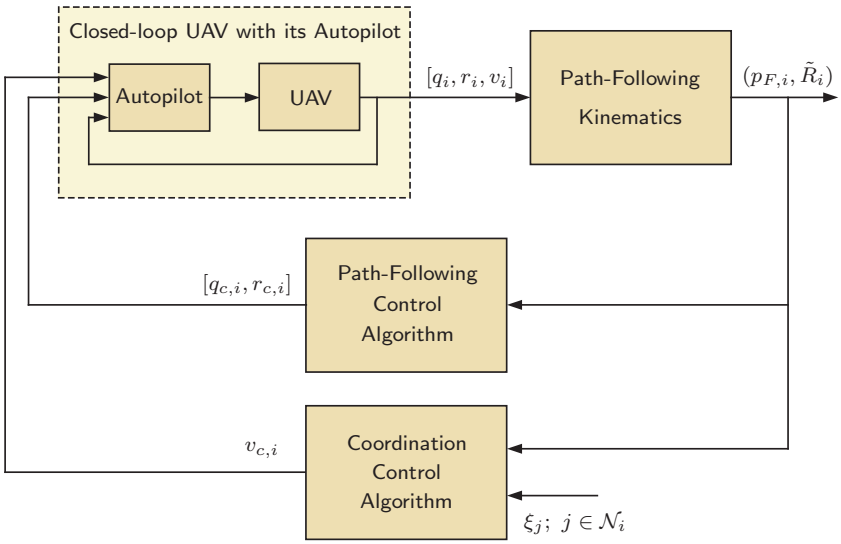

Figure 3: Coordinated path-following closed-loop for the ith vehicle.

It is proven in [36] that, if the connectivity of the communications graph verifies the PE-like condition (6) and the initial conditions are within a given domain of attraction, then there exist control gains for the path-following control law (7)-(8) and the coordination control law (10)-(11) that ensure, first, that the path-following generalized error vector $x_{pf,i}(t)$ of each vehicle converges exponentially fast to a neighborhood of zero; second, that for each pair of vehicles i and j, $i, j \in \{1 \ldots, n\}$, the coordination error $|\xi_i(t) - \xi_j(t)|$ also converges to a neighborhood of zero exponentially fast; and third, that the speed of each UAV satisfies $v_{\min} \leq v_i(t) \leq v_{\max}$ for all $t \geq 0$.

Additionally, it is shown in [36] that the QoS of the network, characterized by the parameters T and μ, limits the achievable guaranteed rate of convergence for the coordination control loop. The results in this paper also imply that, as the parameter T goes to zero and the communications graph becomes thus connected pointwise in time, the convergence rate of the coordination-error dynamics can be set arbitrarily fast by increasing the coordination control gains. This fact is consistent with results obtained in previous work on time-critical cooperative path-following control; see [39, Lemma 2].

Finally, we notice that similar results have been derived for the case of a coordination protocol with multiple leaders [51]; in this case, the convergence rate of the coordination dynamics depends not only on the QoS of the network, but also on the number of leaders. The work reported in [51] also analyzes the convergence properties of protocol (11) when the vehicles exchange quantized measurements, and proves the existence of undesirable "zero-speed" attractors in the presence of coarse quantization.

V. Simulation Results

This section presents simulation results of two cooperative multi-vehicle mission scenarios that show the efficacy of the cooperative framework in this paper. In the first mission, three UAVs must execute a coordinated maneuver to arrive at predefined positions at the same time. We then consider a second mission in which three UAVs must execute sequential auto-landing while maintaining a prespecified safe-guarding separation along the glideslope. Both missions are designed to be executed by small tactical UAVs equipped with an autopilot providing angular-rate and speed tracking capabilities; see Figure 4.

Figure 4: SIG Rascal 110 research aircraft operated by the Naval Postgraduate School for time-critical cooperative missions. Onboard avionics include the Piccolo Plus autopilot, two PC-104 industrial embedded computers, and a wireless MANET link for air-to-air and air-to-ground communications.

A. Path-Following with Simultaneous Arrival

In this mission scenario, three UAVs are tasked to converge to and follow three spatially-deconflicted paths and arrive at their final destinations at the same time. A representative example of such missions is simultaneous suppression of multiple targets located at different positions. Note that this mission imposes only *relative* (rather than *absolute*) temporal constraints on the arrival of the UAVs.

Figure 5 shows the three paths with the parallel transport frames as well as the corresponding desired speed profiles, which assume a final desired speed of 20 $\frac{\text{m}}{\text{s}}$ for all UAVs. The beginning of each path is indicated in this figure with a circle. The figure also shows the coordination maps η_i relating the desired normalized curvilinear abscissa $\ell'_{d,i}$ to the desired mission time t_d. The paths have lengths $\ell_{f1} = 2,084.8$ m, $\ell_{f2} = 1,806.4$ m, and $\ell_{f3} = 2,221.0$ m, and the desired time of arrival is $t_d^* = 85.0$ s. The arrival margin[a] for these trajectories is approximately 31.0 s. Figure 6 presents the path separations, which show a minimum spatial clearance of 125 m, and the desired inter-vehicle separations for this particular mission.

The cooperative motion-control algorithms described in this paper are used to solve this multi-vehicle simultaneous arrival path-following problem. In order to achieve coordination, the UAVs rely on a supporting communications network. The information flow is assumed to be time-varying and, at any given time t, is characterized by one of the graphs in Figure 7.

Simulation results for this particular mission are presented next. Figure 8 illustrates the evolution of the UAVs (blue) as well as the virtual targets (red) moving along the paths (green). This figure also includes the $\mathcal{W}$ frame attached to each UAV (blue) as well as the $\mathcal{F}$ frame attached to the virtual targets (gray). The UAVs start the mission with an initial offset in both position and attitude with respect to the beginning of the framed paths. As can be seen in the figure, the path-following algorithm is able to eliminate this initial offset and steer the UAVs along the corresponding paths, while the coordination algorithm ensures simultaneous arrival at the end of the path at $t = 83.4$ s. Details about the performance of the path-following algorithm are shown in Figure 9; the path-following position and attitude errors, $p_{F,i}$ and $\Psi(\tilde{R}_i)$, converge to a neighborhood of zero within 30 s. The figure also presents the angular-rate commands, $q_{c,i}$ and $r_{c,i}$, as well as the rate of progression of the virtual targets along the path $\dot{\ell}_i$. The evolution of the coordination errors $\xi_i - \xi_j$ and the rate of change of the coordination states $\dot{\xi}_i$ are illustrated in Figure 10, along with the resulting UAV speeds and the integral states of the PI protocol implemented on the follower vehicles. The figure shows that the coordination errors converge to a neighborhood of zero, while the rate of change of the coordination states converges to the desired rate $\dot{\xi}_{\text{ref}} = 1$. In particular, Figure 10b illustrates how the vehicles adjust their speeds (with respect to the desired speed profile) to achieve coordination. Finally, Figure 11 shows an estimate of the QoS of the network, computed as

$$\hat{\mu}(t) := \lambda_{\min}\left(\frac{1}{3}\frac{1}{T}\int_{t-T}^{t} Q_3 L(\tau) Q_3^\top d\tau\right), \qquad t \geq T, \tag{12}$$

with $T = 5$ sec.

[a] *Arrival margin* is a measure of robustness of the generated trajectories at the coordination level; see [43].

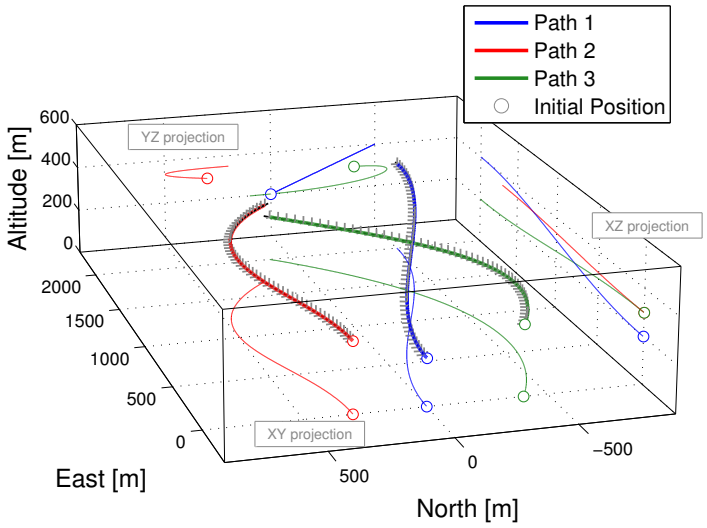

(a) Framed 3D paths

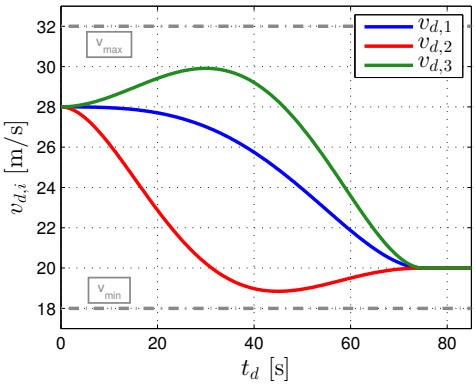

(b) Desired speed profiles

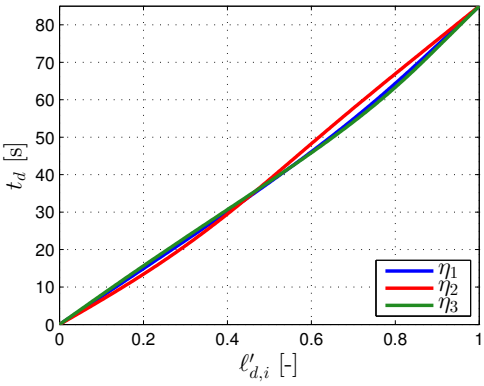

(c) Coordination maps

Figure 5: Path-Following with Simultaneous Arrival. Framed 3D spatial paths along with the corresponding desired speed profiles and coordination maps.

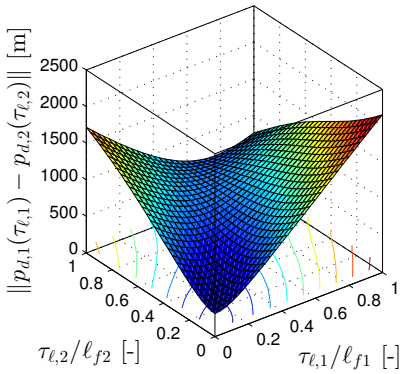

(a) Separation between paths 1 and 2

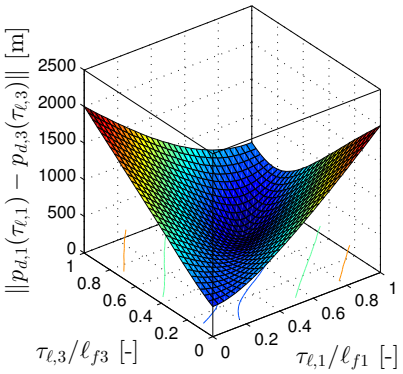

(b) Separation between paths 1 and 3

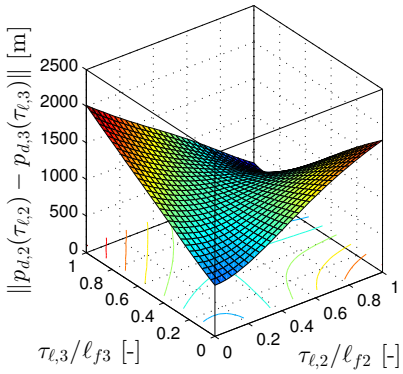

(c) Separation between paths 2 and 3

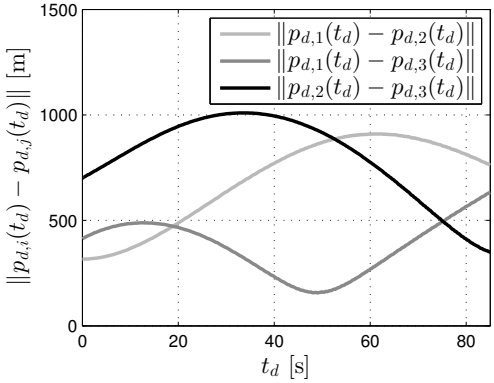

(d) Desired inter-vehicle separation

Figure 6: Path-Following with Simultaneous Arrival. Path separation and desired inter-vehicle separation; the three paths are spatially deconflicted with a minimum clearance of 125 m.

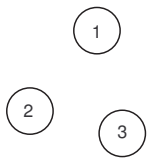

(a) Topology 1

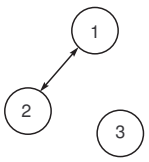

(b) Topology 2

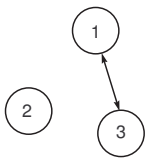

(c) Topology 3

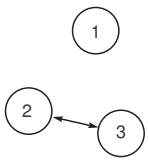

(d) Topology 4

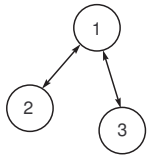

(e) Topology 5

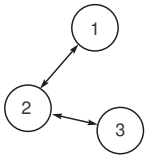

(f) Topology 6

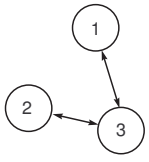

(g) Topology 7

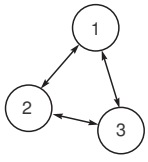

(h) Topology 8

Figure 7: Network topologies. At any given time t, the dynamic information flow is characterized by one of these graphs.

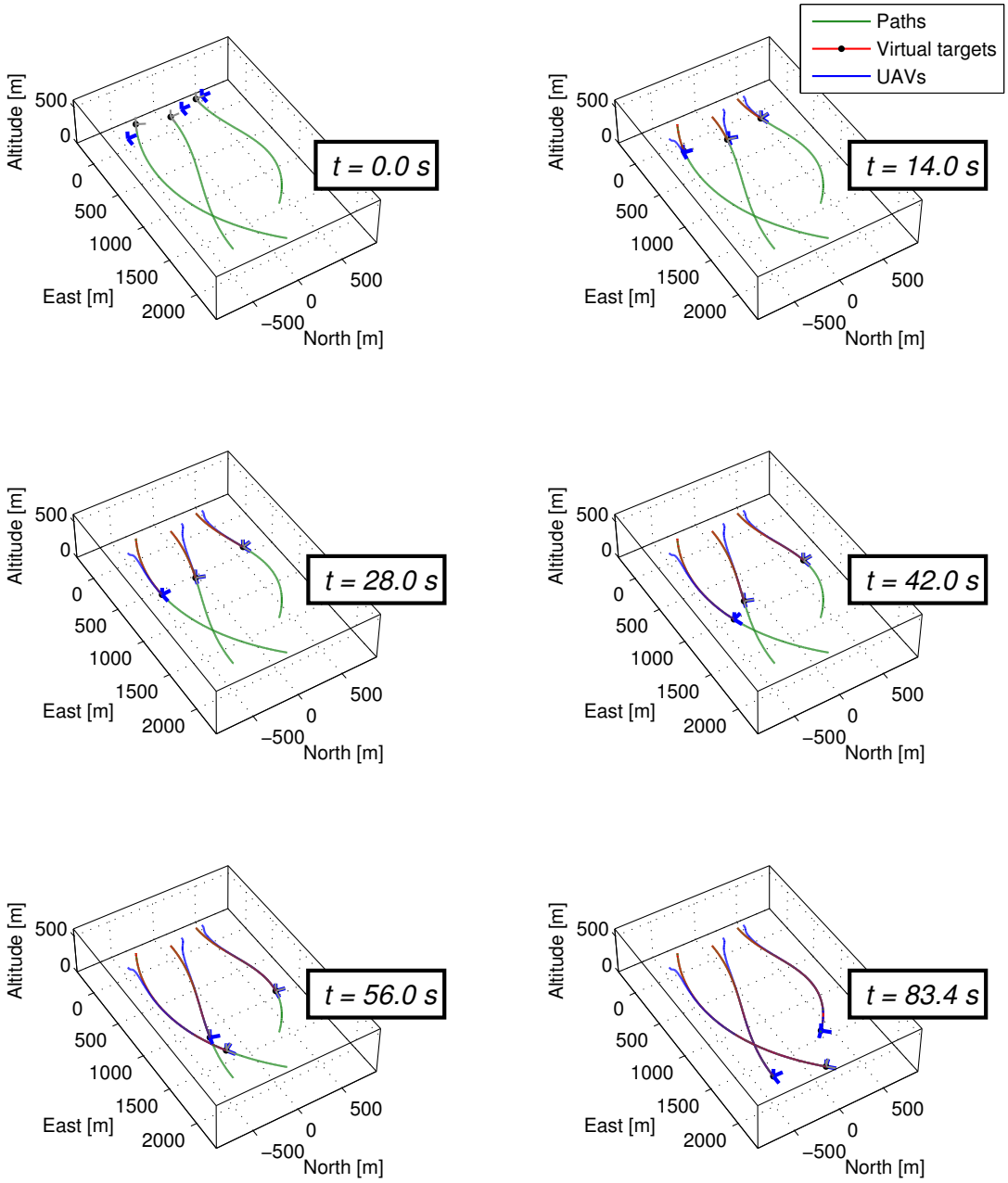

Figure 8: Path-Following with Simultaneous Arrival. The three UAVs achieve simultaneous arrival at their final destinations at $t = 83.4$ s.

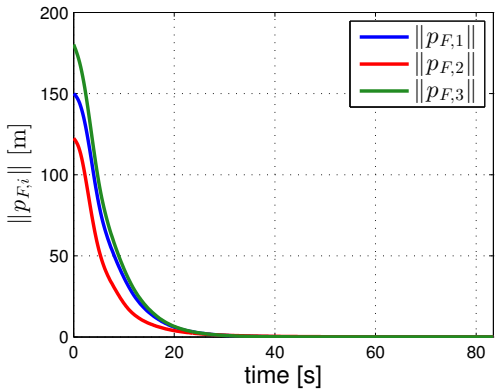

(a) Position error

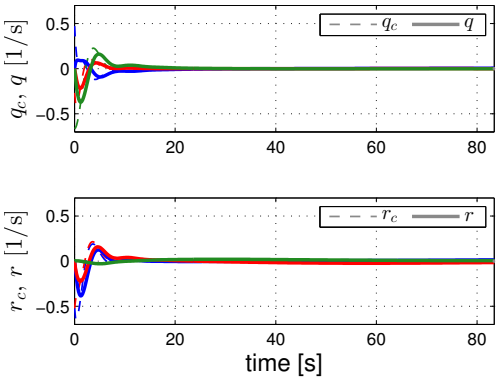

(b) Angular rates

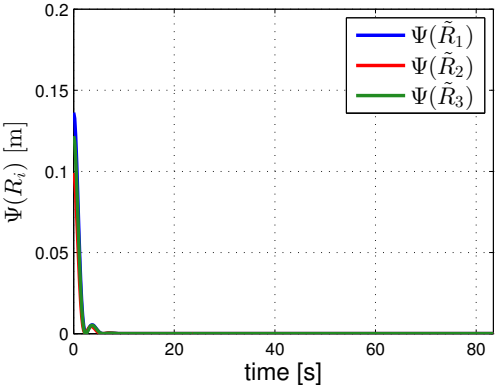

(c) Attitude error

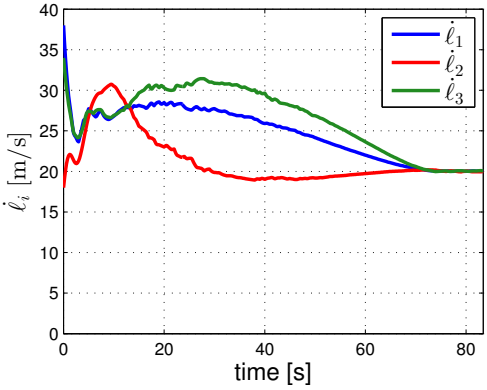

(d) Progression of the virtual targets

Figure 9: Path-Following with Simultaneous Arrival. The path-following algorithm drives the path-following position and attitude errors to a neighborhood of zero.

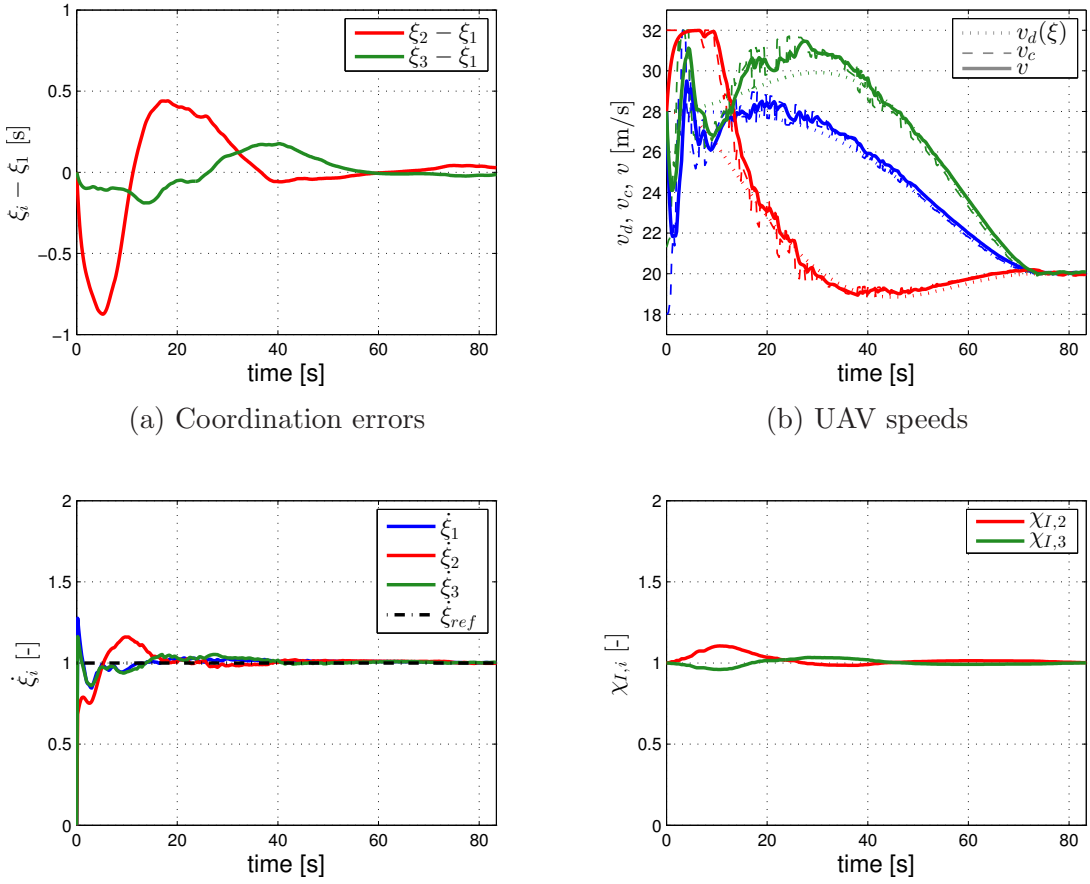

(a) Coordination errors

(b) UAV speeds

(c) Coordination-state rates

(d) Integral states

Figure 10: Path-Following with Simultaneous Arrival. The coordination protocol ensures that the coordination errors converge to a neighborhood of zero and also that the rate of change of the coordination states evolves at about the desired rate $\dot{\xi}_{\text{ref}} = 1$.

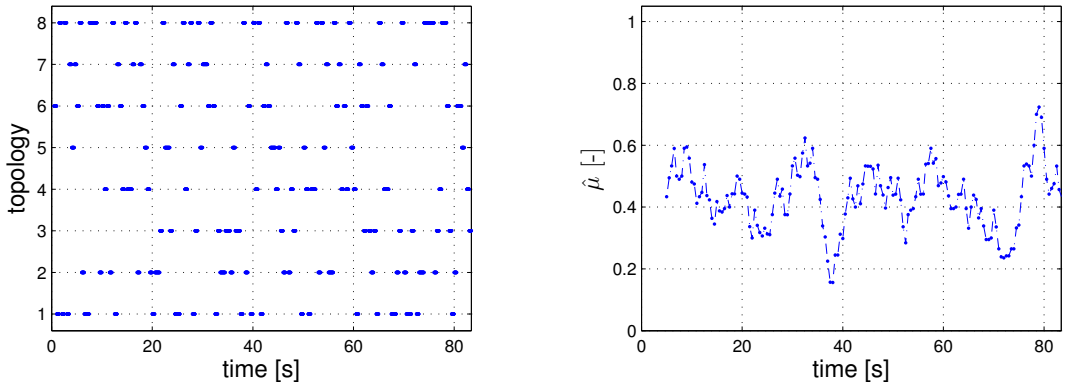

(a) Topology

(b) QoS estimate

Figure 11: Path-Following with Simultaneous Arrival. The graph capturing the time-varying information flow is only connected in an integral sense, and not pointwise in time.

B. Sequential Auto-landing

Here, three UAVs must arrive at the assigned glideslope separated by prespecified safe-guarding time-intervals, and then follow the *glide path* at a constant *approach speed* while maintaining the safe-guarding separation. To this end, time-deconflicted *transition trajectories* are generated from prespecified initial conditions to the beginning of the glide path, satisfying the desired inter-vehicle arrival schedule and taking the UAVs to the desired approach speed. Again, this mission imposes only *relative* temporal constraints on the arrival of the UAVs.

Figure 12 shows the three transition paths with the parallel transport frames as well as the framed 3-deg glide path. The beginning of each transition path is indicated with a circle, while the beginning of the glide path is indicated with a triangle. The figure also presents the desired speed profiles for the initial transition phase that ensure a desired safe-guarding arrival separation of 30 s, trajectory deconfliction, as well as a final approach speed of 20 $\frac{\text{m}}{\text{s}}$. The transition coordination maps are shown in Figure 12c. Finally, the figure also includes the desired speed profile for the approach along the glideslope as well as the corresponding coordination map. The transition paths have lengths $\ell_{f1} = 1,609.0$ m, $\ell_{f2} = 1,962.7$ m, and $\ell_{f3} = 2,836.7$ m, and the desired times of arrival at the glideslope are $t^*_{d1} = 65.0$ s, $t^*_{d2} = 95.0$ s, and $t^*_{d3} = 125.0$ s. The arrival margin for these transition trajectories is approximately 28.8 s. Figure 13 presents the path separations, which show that the three transition paths meet at their end positions (beginning of the glideslope), whereas the desired inter-vehicle separations for this particular mission are never less than 350 m.

The cooperative motion-control algorithms described in this paper can be used to solve this sequential auto-landing problem. In this case, however, since the UAVs are required to maintain a safe-guarding separation during the approach along the glide path, the coordination states have to be redefined as the vehicles reach the glideslope. Hence, while the ith UAV is flying along its transition path, its coordination state is defined as

$$\xi_i(t) = \eta_i(\ell'_i(t)) \,,$$

where $\ell'_i(t)$ is the normalized curvilinear abscissa of the ith virtual target along the corresponding transition path. When the UAV reaches the beginning of the glide path, then its coordination state is (re)defined as

$$\xi_i(t) = \eta_{\text{gs}}(\ell'_i(t)) + t^*_{di} \,,$$

where $\ell'_i(t)$ is now the normalized curvilinear abscissa of the ith virtual target along the glide path, and t^*_{di} is the desired time of arrival of the ith UAV at the glideslope.

Next, we present simulation results for this mission scenario. Figure 14 illustrates the evolution of the UAVs (blue) as well as the virtual targets (red) moving along the paths (green and light blue). Similar to the previous mission scenario, the UAVs start the mission with an initial offset in both position and attitude with respect to the beginning of the transition paths. As can be seen in the figure, the path-following algorithm is able to eliminate this initial offset and steer the UAVs along the corresponding transition paths, while the coordination algorithm ensures that the UAVs reach the glideslope separated by a desired time-interval. The UAVs reach the glideslope at $t = 66.4$ s, $t = 96.2$ s, and $t = 126.2$ s, approximately meeting the desired 30 s inter-vehicle separation. After reaching the glideslope, the path-following algorithm ensures that the UAVs stay on the glide path as the coordination algorithm maintains the desired safe-guarding separation.

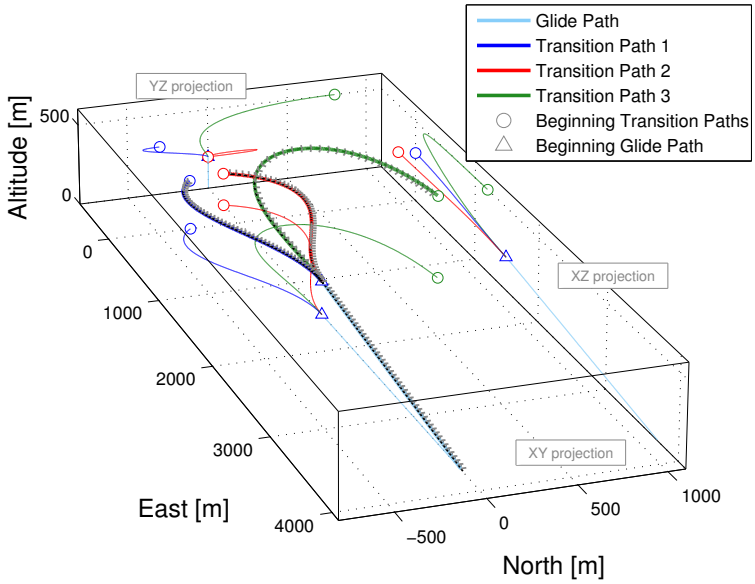

(a) Framed 3D paths

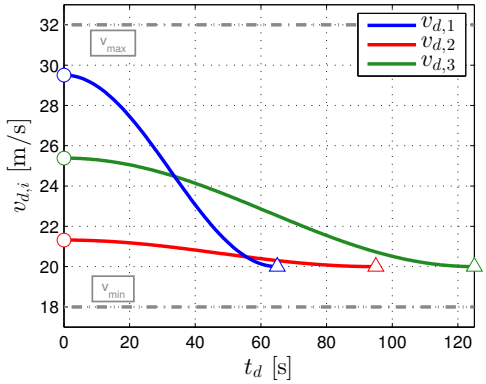

(b) Transition: Desired speed profiles

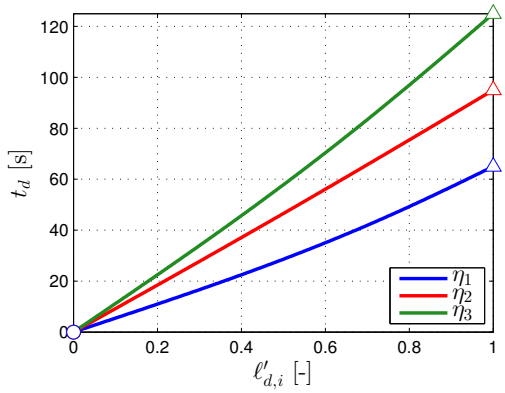

(c) Transition: Coordination maps

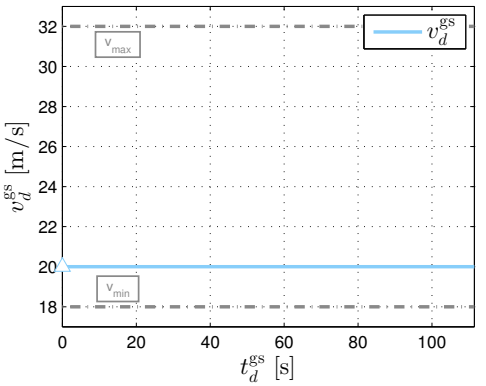

(d) Glideslope: Desired speed profile

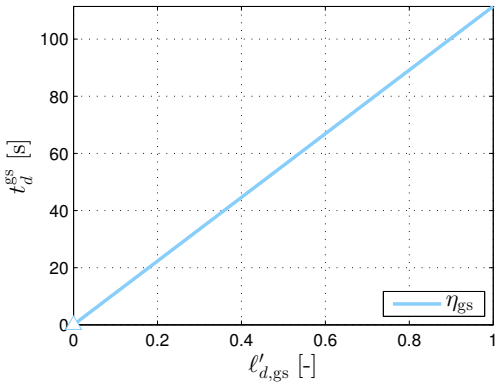

(e) Glideslope: Coordination map

Figure 12: Sequential Auto-landing. Framed 3D spatial paths along with the corresponding desired speed profiles and coordination maps for both the transition trajectories and the glideslope.

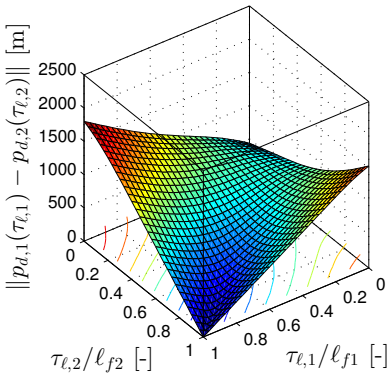

(a) Separation between paths 1 and 2

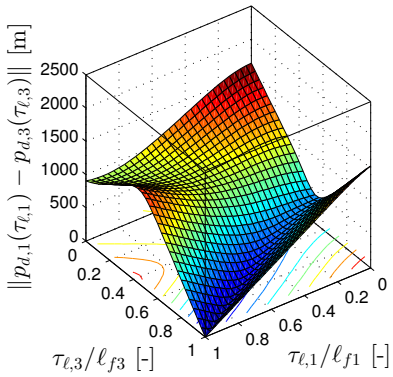

(b) Separation between paths 1 and 3

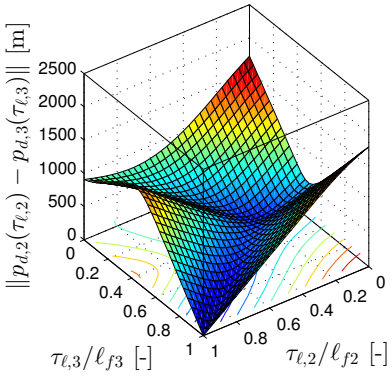

(c) Separation between paths 2 and 3

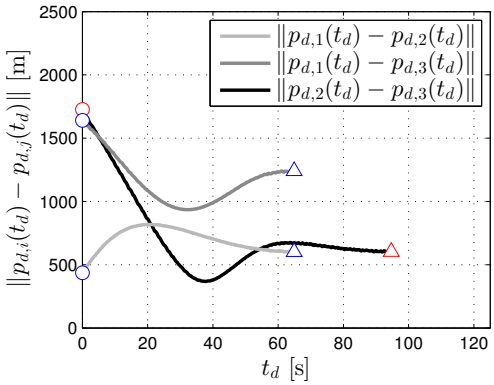

(d) Desired inter-vehicle separation

Figure 13: Sequential Auto-landing. Path separation and desired inter-vehicle separation during the transition phase; the speed profiles ensure deconfliction of the three desired trajectories with a minimum clearance of 350 m.

The simulation is stopped when the first UAV reaches the end of the glide path. Figure 15 shows the path-following position and attitude errors, $p_{F,i}$ and $\Psi(\tilde{R}_i)$, as well as the angular-rate commands, $q_{c,i}$ and $r_{c,i}$, and the rate of progression of the virtual targets along the path $\dot{\ell}_i$. The path-following errors converge to a neighborhood of zero within 40 s. The coordination errors $\xi_i - \xi_j$ also converge to a neighborhood of zero, while the rate of change of the coordination states $\dot{\xi}_i$ converges to neighborhood of the desired rate $\dot{\xi}_{\text{ref}} = 1$; see Figure 16. This figure also shows the UAV speeds and the integral states of the PI protocol implemented on the follower vehicles. In particular, Figure 16b shows that, after an initial transient caused by the initial path-following errors as well as the speed corrections introduced by the coordination protocol, the speed of each UAV converges to its desired speed and, as the vehicles enter the glide path, their speeds converge to the desired approach speed of 20 $\frac{\text{m}}{\text{s}}$. Finally, similar to the previous mission scenario, Figure 17 shows an estimate of the QoS of the network, computed as in (12).

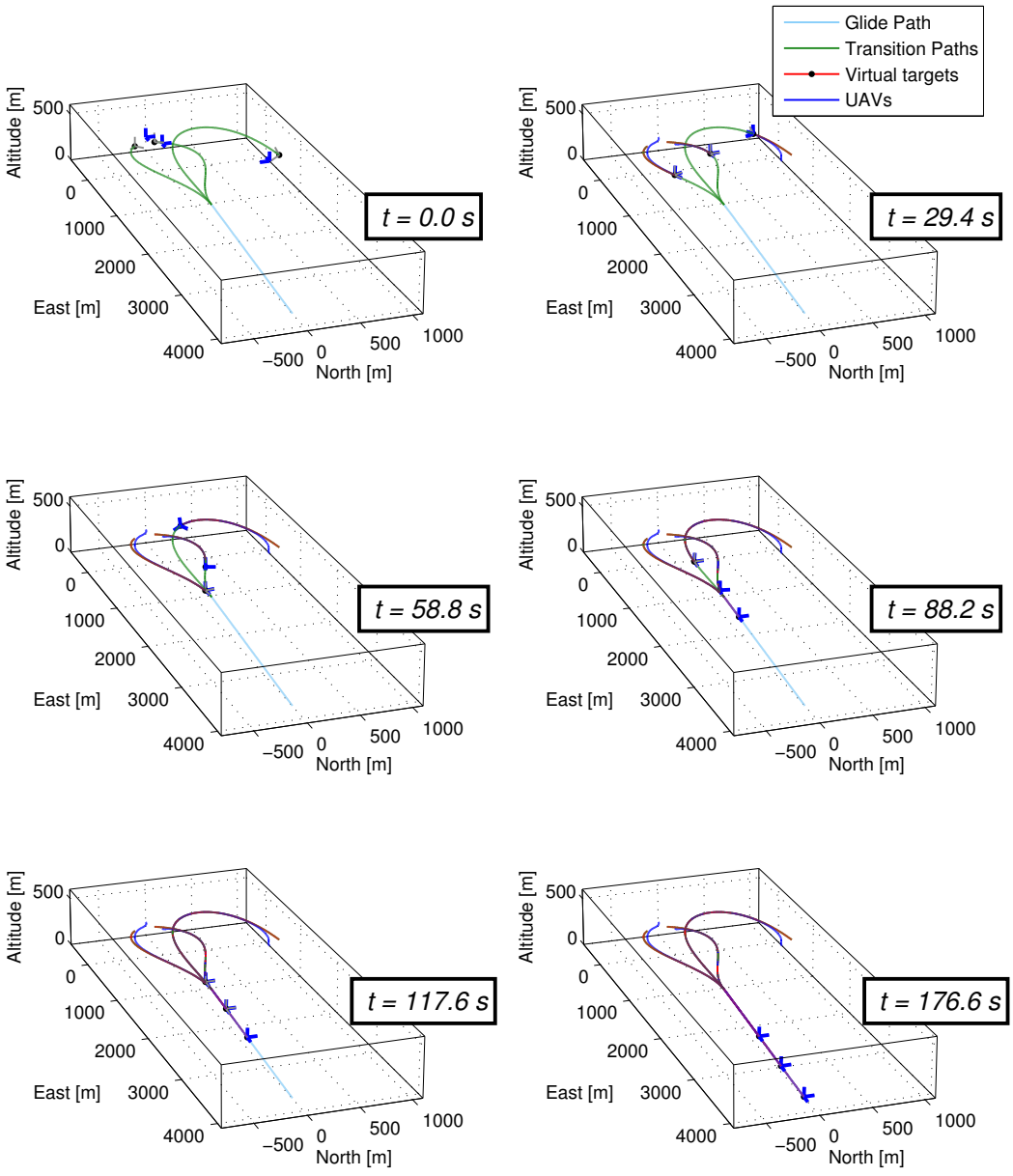

Figure 14: Sequential Auto-landing. The three UAVs arrive at the beginning of the glide path separated by approximately 30 s and maintain this safe-guarding separation as they fly along the glideslope.

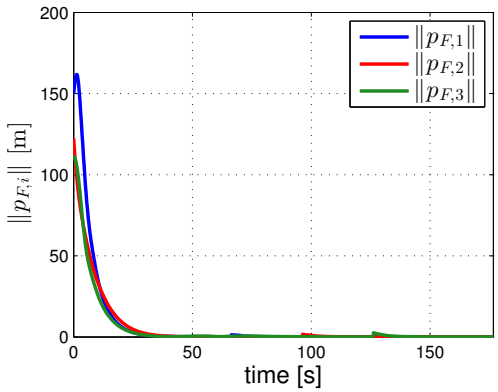

(a) Position error

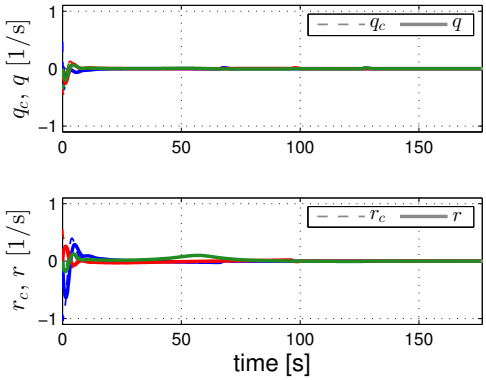

(b) Angular rates

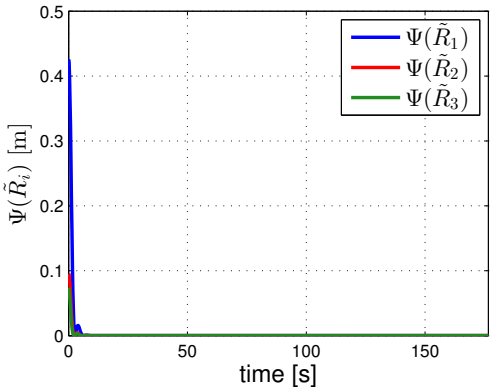

(c) Attitude error

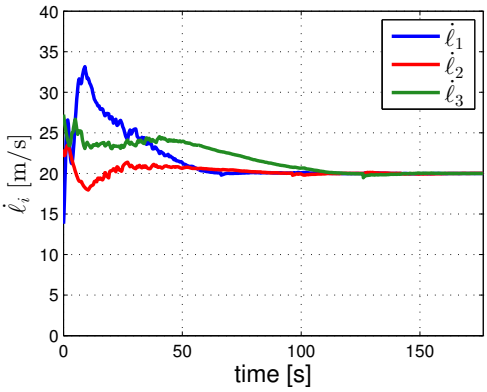

(d) Progression of the virtual targets

Figure 15: Sequential Auto-landing. The path-following algorithm drives the path-following position and attitude errors to a neighborhood of zero.

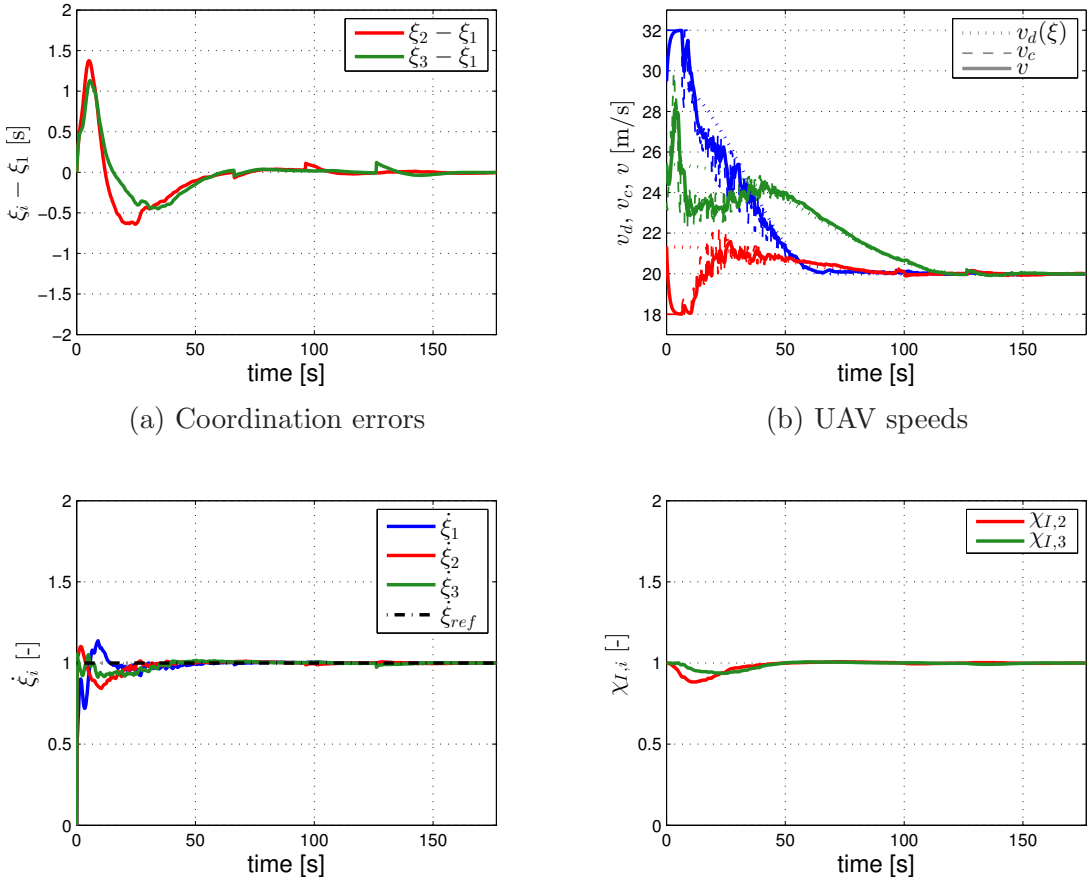

(a) Coordination errors

(b) UAV speeds

(c) Coordination-state rates

(d) Integral states

Figure 16: Sequential Auto-landing. The coordination protocol ensures that the coordination errors converge to a neighborhood of zero, thus ensuring trajectory deconfliction, and also that the rate of change of the coordination states evolves at about the desired rate $\dot{\xi}_{\text{ref}} = 1$.

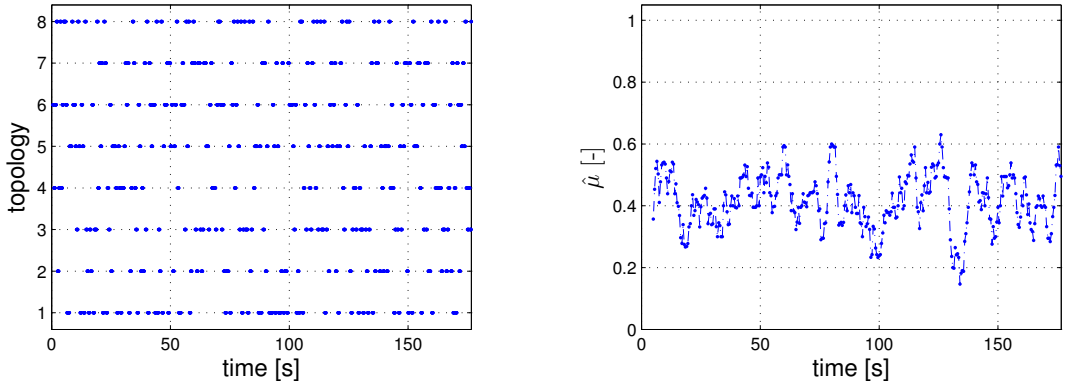

(a) Topology

(b) Quality of service

Figure 17: Sequential Auto-landing. The graph capturing the time-varying information flow is only connected in an integral sense, and not pointwise in time.

VI. Conclusion

The paper presented simulation results of two multi-vehicle time-critical missions that exploit a cooperative control framework proposed by the authors in [36]. The simulation study illustrated the efficacy of the algorithms developed and verified the main theoretical claims. In particular, the results demonstrated that (*i*) at the local level, the proposed path-following control law ensures that every UAV converges to and follows its own path independently of the temporal assignments of the mission; and (*ii*) at the coordination level, the distributed protocol enforces the temporal constraints by adjusting the speed profile of each vehicle based on coordination information exchanged over the supporting communications network.

Acknowledgments

Research was supported in part by U.S. Special Operations Command, U.S. Office of Naval Research, U.S. Air Force Office of Scientific Research, U.S. Army Research Office, European Commission FP7 MORPH Project, and Fundação para a Ciência e a Tecnologia.

Appendix: The *hat* and *vee* maps [52]

The *hat map* $(\cdot)^\wedge : \mathbb{R}^3 \to \mathfrak{so}(3)$ is defined as

$$(x)^\wedge = \begin{bmatrix} 0 & -x_3 & x_2 \\ x_3 & 0 & -x_1 \\ -x_2 & x_1 & 0 \end{bmatrix}$$

for $x = [x_1,\ x_2,\ x_3]^\top \in \mathbb{R}^3$. The inverse of the hat map is referred to as the *vee map* $(\cdot)^\vee : \mathfrak{so}(3) \to \mathbb{R}^3$. The reader is referred to [52] for further details on the hat and vee maps.

References

[1] Tsitsiklis, J. N. and Athans, M., "Convergence and Asymptotic Agreement in Distributed Decision Problems," *IEEE Transactions on Automatic Control*, Vol. 29, No. 1, January 1984, pp. 42–50.

[2] Sepulchre, R., Paley, D., and Leonard, N., *Collective Motion and Oscillator Synchronization*, Vol. 309 of *Lecture Notes in Control and Information Sciences*, Springer-Verlag Berlin, 2005, pp. 189–206.

[3] Jadbabaie, A., Lin, J., and Morse, A. S., "Coordination of Groups of Mobile Autonomous Agents using Nearest Neighbor Rules," *IEEE Transactions on Automatic Control*, Vol. 48, No. 6, June 2003, pp. 988–1001.

[4] Lin, Z., Francis, B. A., and Maggiore, M., "State Agreement for Continuous-Time Coupled Nonlinear Systems," *SIAM Journal on Control and Optimization*, Vol. 46, No. 1, 2007, pp. 288–307.

[5] Egerstedt, M. and Hu, X., "Formation Constrained Multi-Agent Control," *IEEE Transactions on Robotics and Automation*, Vol. 17, No. 6, December 2001, pp. 947–951.

[6] Saber, R. O., Dunbar, W. B., and Murray, R. M., "Cooperative Control of Multi-Vehicle Systems Using Cost Graphs and Optimization," *American Control Conference*, Denver, CO, June 2003, pp. 2217–2222.

[7] Fax, J. A. and Murray, R. M., "Information Flow and Cooperative Control of Vehicle Formations," *IEEE Transactions on Automatic Control*, Vol. 49, No. 9, September 2004, pp. 1465–1476.

[8] Dunbar, W. B. and Murray, R. M., "Distributed Receding Horizon Control for Multi-vehicle Formation Stabilization," *Automatica*, Vol. 42, No. 4, April 2006, pp. 549–558.

[9] Ghabcheloo, R., Pascoal, A. M., Silvestre, C., and Kaminer, I., "Coordinated Path Following Control of Multiple Wheeled Robots using Linearization Techniques," *International Journal of Systems Science*, Vol. 37, No. 6, May 2006, pp. 399–414.

[10] Stevenson, D., Wheeler, M., Campbell, M. E., Whitacre, W. W., Rysdyk, R. T., and Wise, R., "Cooperative Tracking Flight Test," *AIAA Guidance, Navigation and Control Conference*, Hilton Head, SC, August 2007, AIAA-2007-6756.

[11] Keviczky, T., Borrelli, F., Fregene, K., Godbole, D., and Balas, G. J., "Decentralized Receding Horizon Control and Coordination of Autonomous Vehicle Formations," *IEEE Transactions on Control System Technology*, Vol. 16, No. 1, January 2008, pp. 19–33.

[12] Schouwenaars, T., How, J., and Feron, E., "Decentralized Cooperative Trajectory Planning of Multiple Aircraft with Hard Safety Guarantees," *AIAA Guidance, Navigation and Control Conference*, Providence, RI, August 2004, AIAA-2004-5141.

[13] McLain, T. W. and Beard, R. W., "Coordination Variables, Coordination Functions, and Cooperative Timing Missions," *AIAA Journal of Guidance, Control and Dynamics*, Vol. 28, No. 1, January–February 2005, pp. 150–161.

[14] Ousingsawat, J. and Campbell, M. E., "Optimal Cooperative Reconnaissance Using Multiple Vehicles," *AIAA Journal of Guidance, Control and Dynamics*, Vol. 30, No. 1, January–February 2007, pp. 122–132.

[15] Scholte, E. and Campbell, M. E., "Robust Nonlinear Model Predictive Control With Partial State Information," *IEEE Transactions on Control System Technology*, Vol. 16, No. 4, July 2008, pp. 636–651.

[16] Kuwata, Y. and How, J. P., "Cooperative Distributed Robust Trajectory Optimization Using Receding Horizon MILP," *IEEE Transactions on Control System Technology*, Vol. 19, No. 2, March 2011, pp. 423–431.

[17] Fang, L., Antsaklis, P. J., and Tzimas, A., "Asynchronous Consensus Protocols: Preliminary Results, Simulations and Open Questions," *IEEE Conference on Decision and Control*, Seville, Spain, December 2005, pp. 2194–2199.

[18] Mesbahi, M., "On State-Dependent Dynamic Graphs and Their Controllability Properties," *IEEE Transactions on Automatic Control*, Vol. 50, No. 3, March 2005, pp. 387–392.

[19] Stilwell, D. J. and Bishop, B. E., "Platoons of Underwater Vehicles," *IEEE Control Systems Magazine*, Vol. 20, No. 6, December 2000, pp. 45–52.

[20] Stilwell, D. J., Bollt, E. M., and Roberson, D. G., "Sufficient Conditions for Fast Switching Synchronization in Time-Varying Network Topologies," *SIAM Journal of Applied Dynamical Systems*, Vol. 5, No. 1, 2006, pp. 140–156.

[21] Cao, M., Spielman, D. A., and Morse, A. S., "A Lower Bound on Convergence of a Distributed Network Consensus Algorithm," *IEEE Conference on Decision and Control*, Seville, Spain, December 2005, pp. 2356–2361.

[22] Kim, Y. and Mesbahi, M., "On Maximizing the Second Smallest Eigenvalue of State-Dependent Graph Laplacian," *IEEE Transactions on Automatic Control*, Vol. 51, No. 1, January 2006, pp. 116–120.

[23] Mesbahi, M. and Hadaegh, F. Y., "Formation Flying Control of Multiple Spacecraft via Graphs, Matrix Inequalities, and Switching," *AIAA Journal of Guidance, Control and Dynamics*, Vol. 24, No. 2, March–April 2001, pp. 369–377.

[24] Song, Y. D., Li, Y., and Liao, X. H., "Orthogonal Transformation Based Robust Adaptive Close Formation Control of Multi-UAVs," *American Control Conference*, Vol. 5, Portland, OR, June 2005, pp. 2983–2988.

[25] Stipanović, D. M., İnalhan, G., Teo, R., and Tomlin, C. J., "Decentralized Overlapping Control of a Formation of Unmanned Aerial Vehicles," *Automatica*, Vol. 40, No. 8, August 2004, pp. 1285–1296.

[26] Skjetne, R., Moi, S., and Fossen, T. I., "Nonlinear Formation Control of Marine Craft," *IEEE Conference on Decision and Control*, Vol. 2, Las Vegas, NV, December 2002, pp. 1699–1704.

[27] Fossen, T. I., *Marine Control Systems: Guidance, Navigation and Control of Ships, Rigs and Underwater Vehicles*, Marine Cybernetics, Norway, 2002.

[28] Pereira, F. L. and de Sousa, J. B., "Coordinated Control of Networked Vehicles: An Autonomous Underwater System," *Automation and Remote Control*, Vol. 65, No. 7, July 2004, pp. 1037–1045.

[29] Ghabcheloo, R., Aguiar, A. P., Pascoal, A. M., Silvestre, C., Kaminer, I., and Hespanha, J. P., "Coordinated Path-Following Control of Multiple Underactuated Autonomous Vehicles in Presence of Communication Failures," *IEEE Conference on Decision and Control*, San Diego, CA, December 2006, pp. 4345–4350.

[30] Ihle, I.-A. F., *Coordinated Control of Marine Craft*, Ph.D. thesis, Norwegian University of Science and Technology, Trondheim, Norway, September 2006.

[31] Arrichiello, F., Chiaverini, S., and Fossen, T. I., "Formation Control of Marine Surface Vessels using the Null-Space-Based Behavioral Control," *Group Coordination and Cooperative Control*, edited by K. Y. Pettersen, J. T. Gravdahl, and H. Nijmeijer, Vol. 336 of *Lecture Notes in Control and Information Sciences*, Springer-Verlag Berlin Heidelberg, 2006, pp. 1–19.

[32] Breivik, M., Subbotin, M. V., and Fossen, T. I., "Kinematic Aspects of Guided Formation Control in 2D," *Group Coordination and Cooperative Control*, edited by K. Y. Pettersen, J. T. Gravdahl, and H. Nijmeijer, Vol. 336 of *Lecture Notes in Control and Information Sciences*, Springer-Verlag Berlin Heidelberg, 2006, pp. 55–74.

[33] Ihle, I.-A. F., Jouffroy, J., and Fossen, T. I., "Robust Formation Control of Marine Craft using Lagrange Multipliers," *Group Coordination and Cooperative Control*, edited by K. Y. Pettersen, J. T. Gravdahl, and H. Nijmeijer, Vol. 336 of *Lecture Notes in Control and Information Sciences*, Springer-Verlag Berlin Heidelberg, 2006, pp. 113–129.

[34] Kyrkjebø, E., *Motion Coordination of Mechanical Systems: Leader-Follower Synchronization of Euler-Lagrange Systems Using Output Feedback Control*, Ph.D. thesis, Norwegian University of Science and Technology, Trondheim, Norway, April 2007.

[35] Breivik, M., Hovstein, V. E., and Fossen, T. I., "Ship Formation Control: A Guided Leader-Follower Approach," *IFAC World Congress*, Seoul, South Korea, July 2008.

[36] Xargay, E., Kaminer, I., Pascoal, A., Hovakimyan, N., Dobrokhodov, V., Cichella, V., Aguiar, A. P., and Ghabcheloo, R., "Time-Critical Cooperative Path Following of Multiple UAVs over Time-Varying Networks," 2012, Accepted for publication in *AIAA Journal of Guidance, Control and Dynamics*.

[37] Kaminer, I., Yakimenko, O. A., Dobrokhodov, V., Pascoal, A. M., Hovakimyan, N., Patel, V. V., Cao, C., and Young, A., "Coordinated Path Following for Time-Critical Missions of Multiple UAVs via $\mathcal{L}_1$ Adaptive Output Feedback Controllers," *AIAA Guidance, Navigation and Control Conference*, Hilton Head, SC, August 2007, AIAA-2007-6409.

[38] Aguiar, A. P. and Pascoal, A. M., "Coordinated Path-Following Control for Nonlinear Systems with Logic-Based Communication," *IEEE Conference on Decision and Control*, New Orleans, LA, December 2007, pp. 1473–1479.

[39] Aguiar, A. P., Kaminer, I., Ghabcheloo, R., Pascoal, A. M., Xargay, E., Hovakimyan, N., Cao, C., and Dobrokhodov, V., "Time-Coordinated Path Following of Multiple UAVs over Time-Varying Networks using $\mathcal{L}_1$ Adaptation," *AIAA Guidance, Navigation and Control Conference*, Honolulu, HI, August 2008, AIAA-2008-7131.

[40] Ghabcheloo, R., Kaminer, I., Aguiar, A. P., and Pascoal, A. M., "A General Framework for Multiple Vehicle Time-Coordinated Path Following Control," *American Control Conference*, St. Louis, MO, June 2009, pp. 3071–3076.

[41] Ghabcheloo, R., Aguiar, A. P., Pascoal, A. M., Silvestre, C., Kaminer, I., and Hespanha, J. P., "Coordinated Path-Following in the Presence of Communication Losses and Delays," *SIAM Journal on Control and Optimization*, Vol. 48, No. 1, 2009, pp. 234–265.

[42] Kaminer, I., Pascoal, A. M., Xargay, E., Hovakimyan, N., Cao, C., and Dobrokhodov, V., "Path Following for Unmanned Aerial Vehicles using $\mathcal{L}_1$ Adaptive Augmentation

of Commercial Autopilots," *AIAA Journal of Guidance, Control and Dynamics*, Vol. 33, No. 2, March–April 2010, pp. 550–564.

[43] Xargay, E., Dobrokhodov, V., Kaminer, I., Pascoal, A. M., Hovakimyan, N., and Cao, C., "Time-Critical Cooperative Control for Multiple Autonomous Systems," Accepted for publication to *IEEE Control Systems Magazine*, 2012.

[44] Micaelli, A. and Samson, C., "Trajectory Tracking for Unicycle-Type and Two-Steering-Wheels Mobile Robot," Tech. Rep. 2097, INRIA, Sophia-Antipolis, France, November 1993.

[45] Lapierre, L., Soetanto, D., and Pascoal, A. M., "Non-Singular Path-Following Control of a Unicycle in the Presence of Parametric Modeling Uncertainties," *International Journal of Robust and Nonlinear Control*, Vol. 16, No. 10, 2006, pp. 485–503.

[46] Bishop, R. L., "There is More than One Way to Frame a Curve," *The American Mathematical Monthly*, Vol. 82, No. 3, 1975, pp. 246–251.

[47] Hanson, A. J. and Ma, H., "Parallel Transport Approach to Curve Framing," Tech. Rep. TR425, Indiana University Compute Science Department, 1995.

[48] Olfati-Saber, R., Fax, J. A., and Murray, R. M., "Consensus and Cooperation in Networked Multi-Agent Systems," *In Proceedings of the IEEE*, Vol. 95, No. 1, January 2007, pp. 215–233.

[49] Biggs, N., *Algebraic Graph Theory*, Cambridge University Press, New York, NY, 1993.

[50] Arcak, M., "Passivity as a Design Tool for Group Coordination," *IEEE Transactions on Automatic Control*, Vol. 52, No. 8, August 2007, pp. 1380–1390.

[51] Xargay, E., Choe, R., Hovakimyan, N., and Kaminer, I., "Convergence of a PI Coordination Protocol in Networks with Switching Topology and Quantized Measurements," *IEEE Conference on Decision and Control*, 2012, Accepted for publication.

[52] Lee, T., Leok, M., and McClamroch, N. H., "Control of Complex Maneuvers for a Quadrotor UAV using Geometric Methods on $\mathsf{SE}(3)$," *IEEE Transactions on Automatic Control*, 2010, Submitted. Available online: `arXiv:1003.2005v3`.